Journal of Rock Mechanics and Tunnelling Technology (JRMTT)
29 (2) 2023 pp 89-104

Available online at www.isrmtt.com

Analysis of the Evolutionary Characteristics of a Seismically Induced Rockslide by Numerical Modelling Approaches

Deepanshu Shirole, Krishan Gopal Sharma*

Department of Civil Engineering, IIT Delhi, India

**E-mail: dshirole@iitd.ac.in*

ABSTRACT

Rockslides are complex catastrophic events characterized by sudden failure and long runouts involving huge volume of material. Numerical analyses provide a reliable platform for a realistic prediction of their propagation characteristics before the event (e.g., runout distance, velocity, depositional geometry, etc.). The objective of the present study is to verify the reliability of numerical models as used in the simulation of seismically induced rockslides in comparison with the available field measurements. A typical seismic rockslide event has been selected for the numerical analysis in which the rock slope is predominantly divided into two parts: the sliding mass and the stable base block. A discontinuum model of the rock slope is prepared by coupling the discrete blocks of the sliding mass in a continuum-based finite element environment. In addition, the continuum model of the rockslide event is analyzed by the coupled Eulerian-Lagrangian (CEL) method to simulate the large-deformation phenomenon associated with rockslide events. Results show that both modelling methods can produce a reasonable post-failure configuration of the rock slope and agree with previous studies and investigation reports..

Keywords: Rockslide; large deformation; continuum; discontinuum; Lagrangian; Eulerian

1. INTRODUCTION

Landslides denote the movement of a mass of rock, debris, or earth down a slope (Cruden, 1991). Landslides are very complex natural events defined by various processes (progressive slip failure formation, slope collapse, mass runout, rapid flow, etc.) that finally result in the sliding movement of the massive slope-forming material. The triggering reasons for slope instability/eventual failure can be inherent, variable, transient or due to new environmental conditions (Varnes, 1984). Inherent sources may include weakness in the structure of the slope (e.g., weathering, joints, bedding planes, foliations, etc.) (Goel & Mitra, 2015, 2021); variable causes might be short and long-term variation in the groundwater table, snow melting, or heavy rainfall; seismicity is the best example of a transient cause; and changes in environmental conditions (e.g., slope cutting) are often caused by human activity (Varnes,1984). In hilly regions, seismically induced slope instabilities have triggered some catastrophic landslides. Earthquakes cause large-scale ground movement and can trigger severe landslides over broad areas resulting in severe damage and casualties (Harp and Jibson, 1996; Keefer, 2000; Keefer and Larsen, 2007). This is testified by the fact that higher-intensity earthquakes have been observed to trigger thousands of landslides within an area as large as 100,000 km^2 (Keefer, 2000; Keefer and Larsen, 2007). For example, out of the total casualties (90,000) of the 2005 Kashmir earthquake, 30% were victims of seismically induced landslides. The primary issue with such

rockslide events is the high propagation velocity coupled with the massive sliding material volume covering large distances over a short period (Pirulli, 2005). As such, the use of any protective measure against rockslide events is of little significance due to the severity of the phenomenon. Accordingly, zone-based delineation of a region that a rockslide event could potentially influence provides a better solution to safeguard human settlements (prevent fatalities and property damage) against such a natural geohazard. Consequently, it is crucial to understand the propagation mechanisms involved with landslides to realistically predict the areas at risk to a such events and mark settlements away from the sliding block boundaries (Manzella and Labiouse, 2013).

The analysis of the post-collapse propagation characteristics of rock slopes is termed the runout analysis (Zhang et al., 2013). The runout analysis enables a reliable forecast of rockslide propagation characteristics (horizontal runout, total runout, temporal evolution, runout velocity, etc.), which are vital for the appraisal of hazardous areas and for avoiding conservative decisions in the development of an area. Due to the complexities involved in slope geometry, rock characteristics, and flow dynamics concerning a rockslide event, analytical models have limited capabilities to accurately predict rockslide characteristics (e.g., runout distance, propagation velocity, etc.).

Similarly, the rapidly transient and random nature of rockslides makes real-time investigations of a rockslide event extremely challenging and utopian (Manzella and Labiouse, 2013). Accordingly, numerical models are now used routinely in civil engineering applications and academic research to investigate, within realistic geological contexts, the runout of large landslides (Pirulli et al., 2007; Stead et al., 2006). This is because numerical techniques can reasonably account for complications regarding geometry, material anisotropy, non-linear material behaviour and heterogeneity, in-situ stresses and other complex transient processes associated with rockslides.

Numerical models can be broadly classified as a continuum or discontinuum system. Continuum methods demonstrate the advantages of representing the complex geometry of a rock slope as a continuum without any discrete feature (Crosta et al., 2006). Continuum models can also accurately account for the topography effects with a reasonable computational time. The continuum-based models have already been used in many landslide studies, like Kuo et al. (2009), Bozzano et al. (2011), and Liu et al. (2014). Traditional continuum methods typically have a Lagrangian description and so have difficulties in the precise modelling of large deformations due to problems of mesh distortion and mesh entanglement. As a result, continuum-based Lagrangian approaches are currently limited to the estimation of relatively small slope deformations only (Jibson, 2011). The drawback of these methods in dealing with large deformations considerably hinders their application in analyzing rockslides. State-of-the-art modelling techniques based on continuum idealizations have also been employed in synthetic forecasting of the post-failure behaviour of slopes. The coupled Eulerian-Lagrangian (CEL) method can be effectively used, as it can reproduce phenomena associated with large deformations (Qiu et al., 2009). In the CEL (continuum) approach, the significant deformation phenomena are typically characterized by coupling the Eulerian description (for large deformation evaluation) with an updated Lagrangian description. This continuum modelling approach is constrained by the fact that spatial and temporal characteristics of individual rock blocks present in the rock slope cannot be attained, which are important for a rational design of landslide preventive measures (Moormann et al., 2015).

Discontinuum methods, in which the subsurface discontinuities are represented explicitly, can address some of the continuum approach's drawbacks as it allows the modelling of the rock mass as an assemblage of individual rock blocks (Sinha et al., 2020). The dynamic behaviour of each discrete block can be studied by applying constitutive properties, contact laws, and boundary conditions. Furthermore, the discontinuum methods derive the macroscopic behaviour of a system from the emergent microscopic processes, with minimal need for any macroscopic constitutive laws (that may mask some of the micromechanical processes) (Shirole et al., 2020a; Sinha et al., 2020; Sinha & Walton, 2019). Accordingly, the discontinuum methods can realistically model the behaviour of heterogeneous rock slopes (Choi et al., 2015, 2017; Jibson, 2011). Two principal discontinuum methods are the discrete element method (DEM) (Cundall, 1971) and the discontinuous deformation analysis (DDA) (Shi and Goodman, 1989), which differ in the solution procedures that are employed for solving the equation of motion. The primary limitations of conventional discontinuum methods are their low calculation efficiency and difficulty procuring model input parameters, which require excessive experimental calibration. Accordingly, this study attempts to couple the discontinuum modelling approach with the continuum approach, for which the discontinuum model is prepared by modelling the discrete blocks of the rock slope in a continuum FE (finite element) medium, which has the potential to capture the characteristic of the individual rock blocks with a high computational capacity. A purely continuum model, based on CEL approach was also developed to characterize the landslide evolution. Finally, the reliability of discontinuum and continuum models used in landslide propagation analysis is verified by comparing the numerically simulated results. The Daguangbao rockslide, triggered by the 2008 Wenchuan earthquake, has been employed in scientific case study.

2. LANDSLIDE AND EARTHQUAKE CHARACTERISTICS

2.1 The Earthquake of Wenchuan

With a surface wave magnitude (Ms) of 8.0, the earthquake of Wenchuan is regarded as one of the most devastating earthquakes to be recorded in China’s rocky terrains (Zhang et al., 2013). The source of the Wenchuan seismicity is predicted to be present on the Longmenshan fault along the Tibetan plateau (Gorum et al., 2011). This seismicity eventually led to the devastating Wenchuan earthquake along the Longmen Mountain range (Zhang et al., 2013).

This earthquake triggered more than a thousand co-seismic landslides over an area of 0.35 million km^2 in Wenchuan. Crucially, the fatalities due to the seismically triggered landslide activity were estimated to be one-third of the total fatalities (Huang et al., 2011, 2012).

2.2 Daguangbao Landslide

Specifically, the Daguangbao landslide was one of the largest landslides triggered during the Wenchuan earthquake (Zhang et al., 2013). The Daguangbao landslide eventually led to 1.16 billion m^3 of debris accumulation at the slope toe, with a deposition height of 690 m. Figure 1 illustrates the geometry of the Daguangbao slope before the seismic landslide. It demonstrates its elevation decreased from the slope crest to the slope toe by almost 1.5 km over a distance of approximately 3 km. In particular, the Daguangbao landslide represents a sliding phenomenon evolving over weak bedding planes (Zhang et al., 2013). Additionally, the Daguangbao slope can be categorized into three regions (Huang et al., 2011, 2012; Zhang et al., 2013); (i) the Daguangbao peak, in which the slope angle ranges from 50° to 60° with a rock of Permian (P) origin; (ii) second part is the middle

region of the slope with an average angle of 30° has Devonian rocks (D); and (iii) region has a slope angle varying between from 40°-50° (Fig. 2). Furthermore, the foundation rock of the slope is primarily of Sinian origin (Z). For a detailed insight into the geology Daguangbao area, the reader can follow the work of Huang et al. (2011, 2012).

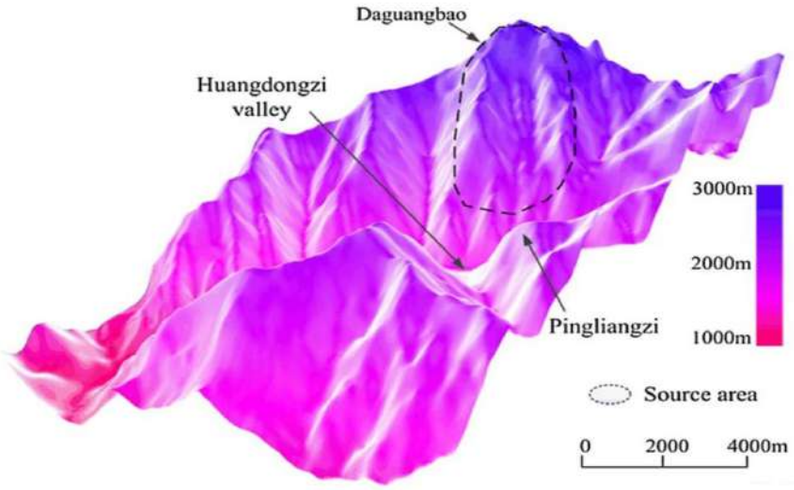

Figure 1 - The topography of the Daguangbao area prior to the landslide activity (Zhang et al., 2013)

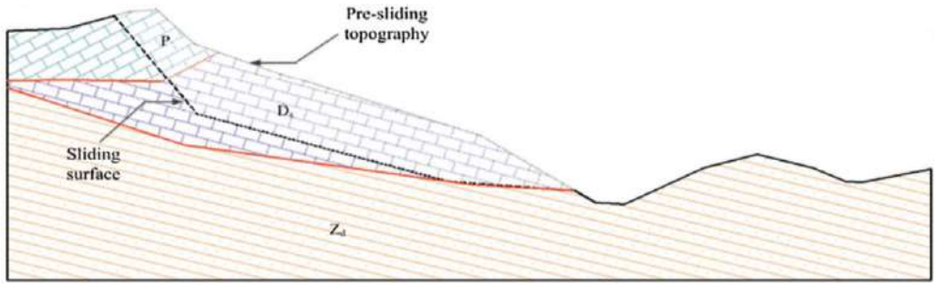

Figure 2 - Geological profile of the Daguangbao rock slope (Zhang et al., 2013)

The Daguangbao area is highly susceptible to seismically induced landslides due to the area's proximity to geological faults. Huang et al. (2011 & 2012) corroborated the existence of past landslide activity in the Daguangbao slope area by referring to the convex nature of the slope and a mild dip in the mid-section area of the slope. A past seismic activity might have initiated the formation of a weak structural plane, which was further disintegrated by the Wenchuan earthquake leading to the slope collapse. Studies carried out by Huang et al. (2011, 2012) and Yueping et al. (2011) approximated the area of influence to be around 10.0km^2. The present study attempts to reproduce the post-failure behaviour of the Daguangbao slope using numerical techniques.

3. NUMERICAL APPROACH- CONTINUUM

3.1 Coupled Eulerian-Lagrangian (CEL) Method

Lagrangian and Eulerian approaches are two different ways to define the motion of a continuum system. A Lagrangian description takes the material configuration (undeformed) as the initial frame

of reference. In Lagrangian, FEA (finite element analysis) nodes are coincident with the material points, making accurate modelling of large deformation inefficient (Kafaji, 2013). Relative to this, the Eulerian description employs spatial coordinates to monitor the evolution of motion and modulations in the physical characteristics of a continuum mass at discretely defined points in space. Specifically, it utilizes the spatial configuration as the initial reference (ABAQUS, 2014). The motion and deformation of the Eulerian material (as it flows) are typically computed by the calculation of the Eulerian Volume Fraction (EVF). Each Eulerian mesh element is provided with a percentage, representing the fraction of the element filled with the continuum. The combination of Lagrangian and Eulerian descriptions results in the so-called Coupled Eulerian-Lagrangian technique. CEL makes it plausible to simulate large deformation phenomena by coupling the best aspects of Lagrangian and Eulerian descriptions. Figure 3 demonstrates the CEL model of the Daguangbao slope prepared in the commercial software ABAQUS (2014), which has the capability of CEL analysis.

The CEL approach uses the Penalty contact method as the contact formulation. Contact coupling occurs between Lagrangian slave nodes and Eulerian master nodes. Specifically, the contact condition is defined by the penetration of the Lagrangian body (structure) onto the Eulerian body (fluid) (Moormann et al., 2015). The degree of penetration (d^{n+1}) is computed from the relative velocity between the slave ($v_s^{n+\frac{1}{2}}$) node and master ($v_m^{n+\frac{1}{2}}$) node at each time step, Δt, as per Eq. 1.

$$d^{n+1} = d^n + \left(v_s^{n+\frac{1}{2}} - v_m^{n+\frac{1}{2}} \right) \cdot \Delta t \tag{1}$$

where v_s and v_m are the slave and master node velocities, respectively, and d is the penetration depth. The superscript (n) refers to the increment number. The contact force, F between the Lagrangian body and the Eulerian material is given by Eq. 2.

$$F = k \cdot d \tag{2}$$

where factor k depends on the stiffness of the two bodies in contact.

4. NUMERICAL APPROACH - DISCONTINUUM

Discontinuum models have been successfully used in the study of landslides by Wu and Chen (2011), Kveldsvik et al. (2009), Hatzor and Feintuch (2001) and many others. Distinctively, in the present research, a discrete model of the slope is prepared by coupling it with a continuum FE medium, for which the sliding mass of the Daguangbao rock slope is discretized into an assemblage of individual continuum rock blocks. The assemblage of each rock block is based on the orientation of pre-existing discontinuities in the rock slope (Zhang et al., 2013). The base block of the rock slope is assumed to be a stable elastic continuum body. Figure 4 shows the 3D discrete model of the Daguangbao slope having 634 continuum blocks. The discrete model is simulated for the seismic rockslide event by the dynamic explicit finite element technique. It is to be noted that the work conducted by Zhang et al. (2013) was based on the discontinuum deformation analysis (DDA), which is an explicit discontinuum modelling method. In relation to this, the present technique is the pseudo continuum-discontinuum method, in which the material rotation and separation is novelly modelled through a continuum-based platform, significantly redcuing the computational time and cost.

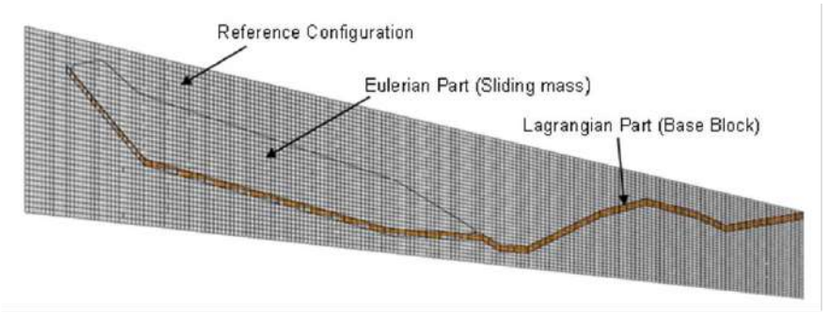

Figure 3 - The continuum description of the Daguangbao slope as per the CEL approach

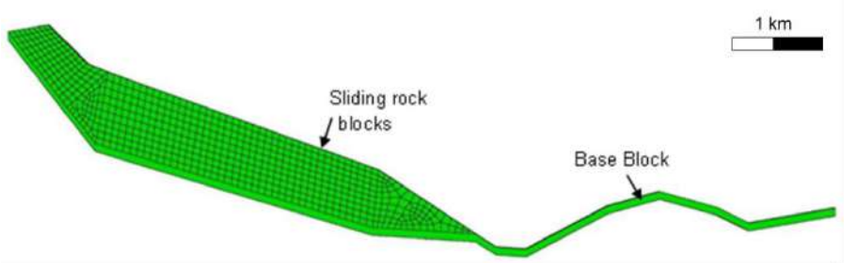

Figure 4 - 3D Discrete model of the Daguangbao rock slope

5. NUMERICAL ANALYSIS

The general approach used in the research is to perform numerical simulations using the multi-physics ABAQUS (2014) finite element package. The ABAQUS framework enables the creation of individual parts of a model, and the assembly of these parts gives the model's overall geometry (ABAQUS, 2014). Contact modelling specifies the interaction and the force transfer mechanisms between each of these individual parts. In the mechanical contact algorithm, interaction procedures in normal and tangential directions to the surfaces in contact are specified. Normal behaviour defines the surface behaviour in the normal direction to the surface, while tangential behaviour characterizes the relative tangential motion between interacting surfaces. The normal and tangential stresses in ABAQUS follow the classical isotropic Coulomb friction model for defining slip contact (ABAQUS, 2014). Before modelling the Daguangbao slide, the contact algorithm of ABAQUS was verified using a simple block model.

5.1 Simple Block Model

A simple block, as shown in Figure 5, is numerically analyzed, for which a rectangular sliding block of 10 m length, 5 m height and unit thickness is placed over a triangular base block having an angle of inclination (α) of 30°. Each of the two blocks has a unit weight (γ) of 26 kN/m^3, Young's modulus (E) of 1.8 GPa and Poisson's ratio (ν) of 0.1. Theoretically, for frictional contact, the limiting equilibrium state is attained at a critical value of friction coefficient (μ_{crit}) for a specified angle of inclination per Eqs. 3 and 4.

$$W \sin \alpha = R = \mu \cdot W \cos \alpha \tag{3}$$

$$\mu_{crit} = \tan^{-1}(\alpha) \tag{4}$$

where W is the weight of the sliding block, R is the resisting force against sliding, μ is the coefficient of friction, and α is the angle of inclination. The 3D numerical model of the sliding block is shown in Figure 5. The length of the linear 10-noded tetrahedron meshing elements is set as unity in the out-of-plane direction (Z-axis). In the analysis, the friction coefficient was reduced in steps, and the corresponding equilibrium state was verified at the end of each step. The simulation was performed for three values of friction coefficients: 0.60, 0.59 and 0.58. As calculated from Eq. (4), the critical inclination angle is 30°.

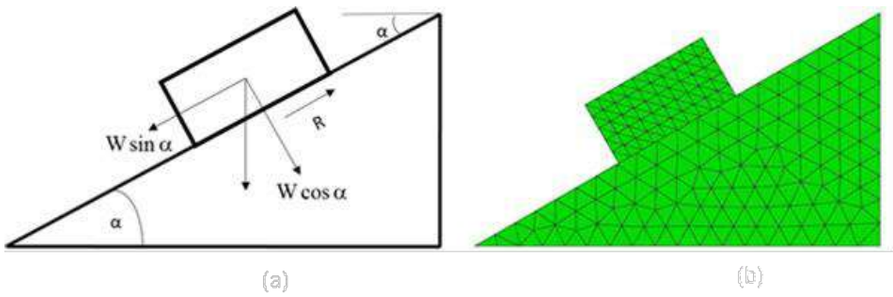

Figure 5 - Sliding block model: (left) mathematical (right) numerical model

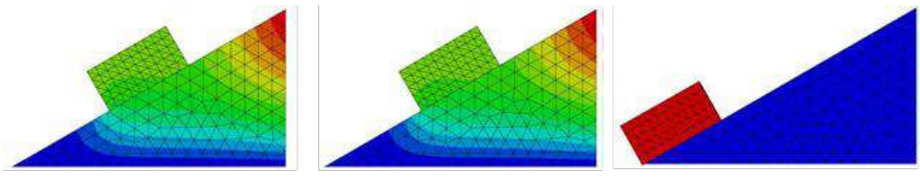

Figure 6 - Position of the block after sliding with different friction coefficients μ: (left) 0.60, (middle) 0.59, and (right) 0.58

Figure 6 shows the position of the block at the end of the analysis for each value of the friction coefficient. The sliding block fails at a friction coefficient of 0.58, giving a 0.52% mathematical error when compared to the theoretical value of the critical friction coefficient (0.577). This minor error can be attributed to the approximate nature of the finite element formulation and can be neglected. These results testify to the reliability of the ABAQUS contact algorithm in the modelling of the interaction between assembled bodies.

5.2 Solution Procedure

Transient loading due to seismic vibrations necessitates dynamic analysis for a reliable response prediction. Furthermore, the nonlinearity in a system resulting from loading conditions, geometry, or material behaviour can be simulated using dynamic non-linear analysis techniques. Incremental time-marching schemes have to be used for studying the non-linear response of a system. For this purpose, ABAQUS has a dynamic explicit integration scheme which is well-suited to simulate brief transient dynamic events such as impact loading and sudden shocks problems (Gorum et al., 2011). For each increment, the program involves the solution of the dynamic equilibrium (Eq. 5).

$$M\ddot{u} = F_{ext} - F_{int} \tag{5}$$

where, M is the mass matrix, $\ddot{u}$ is nodal acceleration while F^{ext} and F_{int} are the external and internal force vectors, respectively. Velocity, $\dot{u}$ and displacement, u at the next increment $(t + \Delta t)$ is calculated by integration of acceleration and velocity over time (t) using the central difference time marching scheme per Equations 6 and 7:

$$\dot{u}|_{\left(t+\frac{\Delta t}{2}\right)} = \dot{u}|_{\left(t-\frac{\Delta t}{2}\right)} + \frac{\left(\Delta t|_{(t+\Delta t)} + \Delta t|_{(t)}\right)}{2} \ddot{u}|_{(t)} \quad (6)$$

$$u|_{(t+\Delta t)} = u|_{(t)} + \Delta t|_{(t+\Delta t)} \cdot \dot{u}|_{\left(t+\frac{\Delta t}{2}\right)} \quad (7)$$

In the explicit approach, typically, a lumped mass matrix is employed for the computation of the equations of acceleration, terminating the requirement to solve individual sets of equations. Consequently, there is no need for global matrices, which significantly reduces the computation time (Moormann et al., 2015). It can also simulate complicated contact conditions and large deformations along with high-speed dynamic conditions (Xu et al., 2013). Landslide runout is a large deformation problem known to be comprised of rock block motion, separation, impact, and other complicated contact problems. The ABAQUS/Explicit numerical solver, therefore, is an appropriate solution procedure for studying the propagation mechanism of landslides and has been used in numerical analysis (ABAQUS, 2014).

5.3 Material Properties

For the Daguangbao slide, the sliding mass is comprised of rocks from the Permian and Devonian groups (Figure 2). But for ease of analysis, it is assumed that the sliding mass is made up of the Devonian group only. This presupposition is justified by the fact that the Daguangbao slope is predominantly Devonian-type rock and hence will not have a significant effect on the simulated results. Table 1 gives the values of the Hoek-Brown (Hoek & Brown, 1988) input parameters from which the rock mass strength parameters have been obtained (Zhang et al., 2013). For simplifying the numerical computation, individual rock blocks in the discrete model of the slope are considered to be elastic (Xu et al., 2013). The interaction between the blocks is defined by the Mohr-Coulomb model. In the CEL continuum model, sliding mass, which constitutes a jointed rock mass, is modelled as an equivalent continuum having a mass density, Υ of 0.026 MN/m^3, Elastic Modulus, E of 2630 MPa and Poisson's ratio, v of 0.2 (Zhang et al., 2013). Rock joint strength parameters significantly affect rock mass behaviour, so these parameters are directly used to define the Mohr-Coulomb shear strength parameters of the continuum sliding mass. Values adopted for cohesion (c) and friction angle (ϕ) in joints are 1.576 MPa and 12.2°, respectively, per the study of Zhang et al. (2013).

Table 1 - Input parameters of the Hoek-Brown criterion (Hoek and Brown, 1988)

	σ_{ci} , MPa	GSI	m_i	γ , kN/m^3	D
Sliding mass	43.8	40	9	26	1
Base block	87.2	70	7	26	1

Notations: σ_{ci} - *uniaxial compressive strength of intact rock; GSI – Geological Strength Index; γ density of rock mass; D-disturbance factor*

Table 2 - Mohr-Coulomb strength parameters for Daguangbao slope (Zhang et al., 2013)

	σ_t, kPa	c, MPa	ϕ	E, GPa	v
Sliding mass	32	1.576	12.2°	2.63	0.2
Base block	556	4.52	23.53°	14.76	0.1

Notations: σ_t *- tensile strength of intact rock; c – cohesive strength;* ϕ*-angle of internal friction; E-modulus of elasticity;* v*-Poisson's ratio*

5.4 Boundary Conditions

In the CEL model, the material undergoing large deformations (debris flow) is analyzed as a Eulerian body, while the stable particles/systems are given a Lagrangian description (base block). The base block of the slope in the CEL model is meshed by the regular 8-noded hexahedron elements under Lagrangian descriptions. These elements are also used for meshing the discrete model's rock blocks.

In the numerical models of the rock slope, a plane strain condition is implemented by restraining the slope from deforming in the out-of-plane direction (Z-axis). In the simulation stage for initializing the gravitational stresses, the base block is also retrained from movement along the in-plane (X,Y) directions. During the earthquake vibration stage, seismic motions on the base block are applied by using the concept of a shake table experiment, where vibrations are imposed by applying a transient boundary condition on the table. Figure 7 shows the velocity time-history of the Wenchuan earthquake, which is essentially a projection combination in the main sliding direction (Zhang et al., 2013) (Eq. 8).

$$v_{slide} = v_{e-w} \cdot sin60^\circ + v_{n-s} \cdot cos60^\circ \quad (8)$$

where, v_{slide} is the velocity of the Wenchuan earthquake in the direction of sliding, v_{e-w} is seismic velocity along the East-West direction in a horizontal plane, while v_{n-s} seismic velocity along the North-South direction in a horizontal plane. The dip direction of the Daguangbao slope is 60° North.

5.5 Numerical Simulations

To provide accurate results, the 3D numerical model of the rock slope must reflect the actual geological characteristics of the slope, in practice, the degree to which this can be achieved must be balanced with the computational time. Based on the geological characteristics and site investigation data of the Daguangbao area, the thickness of the rock slope in the out-of-plane direction is taken as 50m. The thickness of the mesh elements is set equal to the thickness of the rock slope in the Z-direction to have a uniform stress distribution in the out-of-plane direction. Because of this, it became possible to simulate a 2D case using a 3D numerical formulation.

The analysis for both numerical approaches is performed in two steps. Initially, the quasi-static solution for the gravitationally induced stress condition is obtained. In the loading phase, seismic excitations are given to the base block as a transient boundary condition. Corresponding to the time history of the Wenchuan earthquake, the first 60 seconds of the seismic history is used in this study. The simulation, in total, is carried out for 100 seconds.

The effect of joint frequency on the propagation mechanism of a rockslide is also studied in the present paper with the help of the coupled discontinuum-continuum model. The joint frequency study

is carried out by varying the intensity of joints in the rock mass of the slope. Figure 8 depicts the high, medium and low joint frequencies in the sliding rock mass.

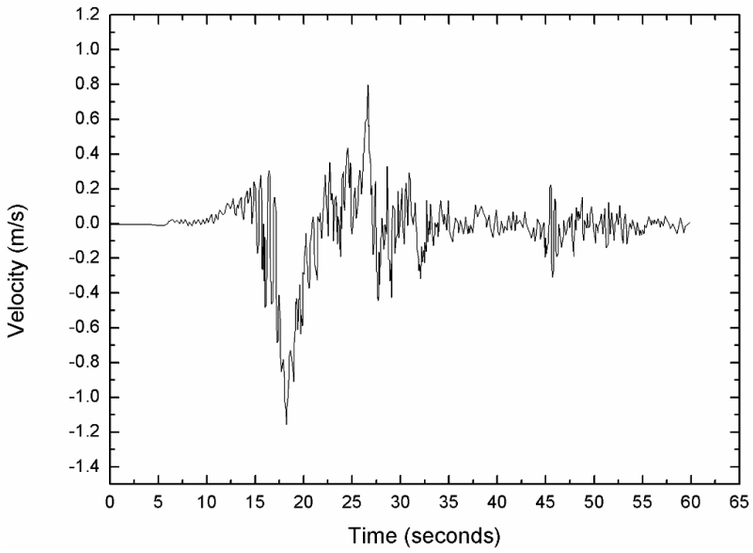

Figure 7 - Horizontal Velocity-time history of the Wenchuan Earthquake (Zhang et al., 2013)

6. RESULTS

After modelling the initial equilibrium state of the Daguangbao rock slope, the post-failure propagation characteristics of the slope are analyzed under the influence of seismic excitations. The kinetic energy of the system is examined to ascertain the state of equilibrium in the pre-failure stage, after which seismic vibrations are given to the base block to actuate slope collapse. Figure 9 shows the Daguangbao rockslide propagation as simulated from the discrete model. Flow characteristics of the rockslide reproduced by the CEL-continuum model are illustrated in Figure 10.

During the earthquake vibrations, the stress state of the slope may have been modified, leading to slope collapse and an eventual landslide. In the first 30 seconds, the landslide moved about 650m at approximately 80km/h. As the seismic vibration reduces (at about 60s), the kinetic energy of the landslide also decreases (Figs. 9-10). Finally, the sliding mass crossed Huangdongzi valley and ran up to the opposite side. The crushing of rock mass may have caused a reduction in the rock material's frictional strength, causing high slide velocity during the initial stage of the landslide. Some of the rock mass material even fell back and formed an accumulation in the valley with a height of 600m, agreeing with the field observations.

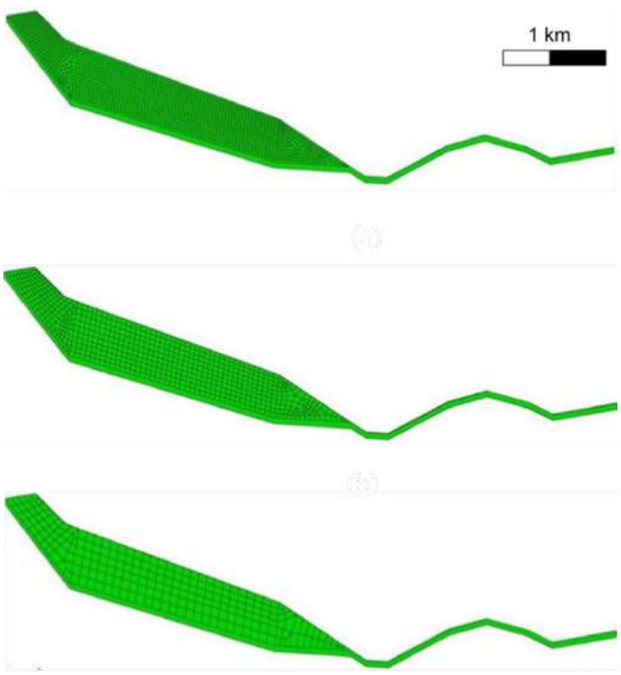

Figure 8 - Daguangbao rock slope with high joint frequency (top), medium joint frequency (middle), and low joint frequency (bottom)

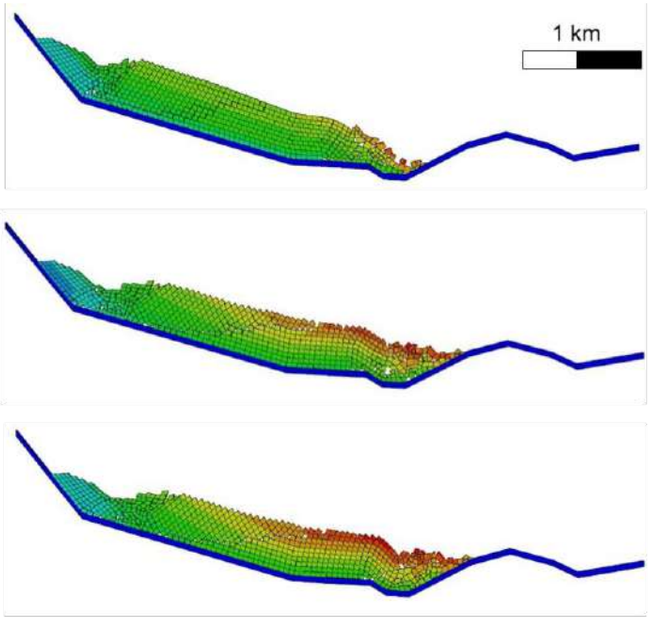

Figure 9 - Runout of the Daguangbao rockslide from the coupled discontinuum-continuum model at (top) 30 seconds, (middle) 50 seconds, and (bottom) 100 seconds

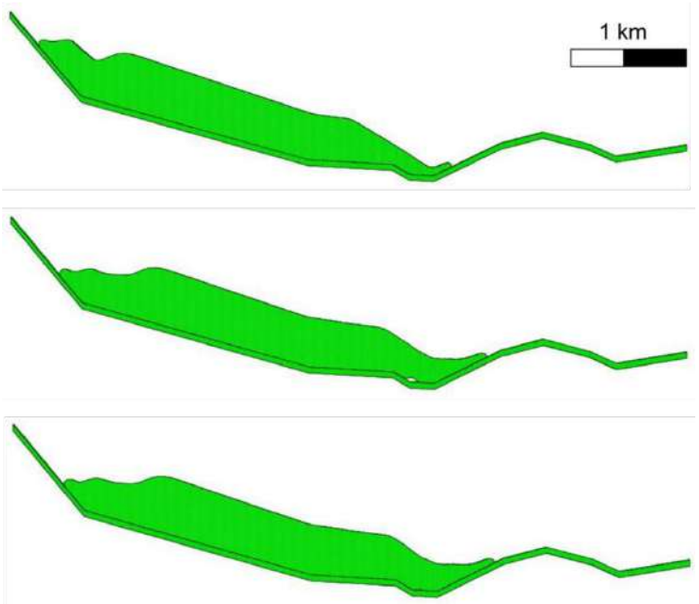

Figure 10 - Runout of the Daguangbao rockslide from the CEL continuum approach at (top) 30 seconds, (middle) 50 seconds, and (bottom) 100 seconds

The horizontal runout distance is noted for both the numerical approaches at 30 seconds, 50 seconds and 100 seconds. The impact of joint frequency on the rockslide runout is depicted in Figure 11. Simulated results show that the sliding blocks climb over the valley at the slope toe.

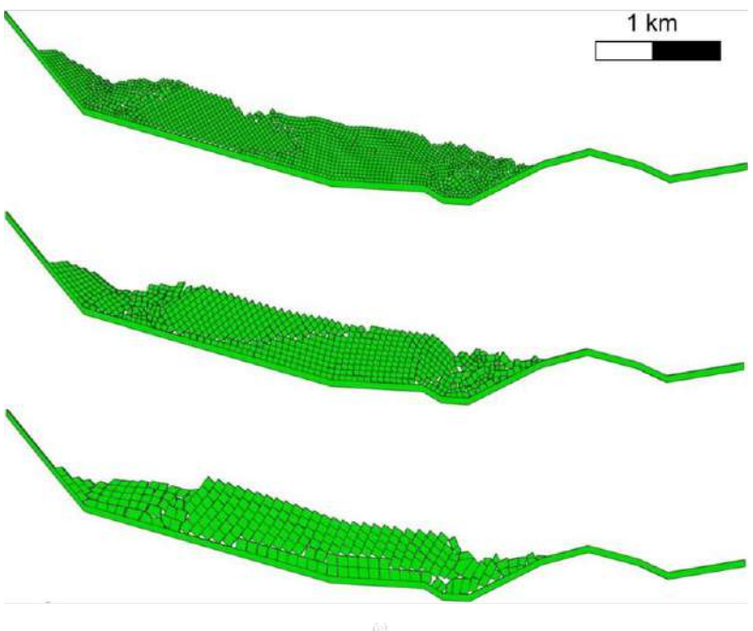

Figure 11 - Rockslide runout with high joint frequency (top), medium joint frequency (middle) and low joint frequency (bottom)

Table 3 - Runout from the numerical models

Numerical Model	Horizontal runout (m)		
	30 seconds	50 seconds	100 seconds
CEL-continuum	539	805	850
Discrete	657	905	932

Table 4 - Runout from the discrete model with varying joint frequency

Joint Frequency	Runout of the discrete model with regular joint orientation (m)		
	30 Seconds	50 Seconds	100 Seconds
High	603	805	901
Medium	657	905	932
Low	491	780	840

In the DDA analysis carried out by Zhang et al. (2013), the runout of the Daguangbao landslide computed at 30 seconds, 50 seconds and 100 seconds is 657 m, 824 m and 944 m, respectively. The values of the rockslide runout computed from the discrete and continuum modelling techniques, as developed in this study, are given in Table 3. The final runout distance of 932 m obtained from the developed discrete model generally agrees with the results (944m) achieved by DDA discontinuum modelling by Zhang et al. (2013). The slight variations in the magnitudes of the runout as simulated via the DDA analysis of Zhang et al. (2013) and by the numerical approach developed in this work can be associated with the fact that DDA is an implicit discrete element method. Relative to this, the discontinuum approach developed in this study is fundamentally based on continuum-based idealizations.

In addition, the final toe displacement of the rockslide given by the CEL continuum model is 850 m (Table 3). It is on the lower side of the reference solution given by Zhang et al. (2013) and the discontinuum approach developed in this study. The CEL runout varies from the reference runout distance and runout obtained from the discrete model of the present study by 9.9% and 8.8%, respectively. The final displacement of the continuum model varies from that of the discrete model because, unlike discrete models, the dilatant phenomena of block toppling, block rotation and block detachment cannot be simulated in continuum models. Also, shear failure occurs along the joints in a discrete model, while the continuum model has an internal shear failure, with the former amplifying the effect of shear strength on the rock mass behaviour. Nevertheless, from Figures 9 and 10, it can be concluded that the post-failure geometry of the rockslide simulated from the continuum and discrete models is quite similar.

In addition to this, runout values from the discrete model of the rock slope for different joint frequencies were also assessed, as given in Table 4. It shows that the slopes with high joint frequencies have considerably increased runout distance relative to slopes with lesser degrees of joint frequencies. From the analyses of discrete models with, it is found that low joint frequency gives the least slope runout of 840 m (Table 5). This is likely because the rock mass is less fragmented, and the big rock blocks at the toe hamper the movement of the blocks behind them (Figure 11). The model with high joint frequency gives runout (901 m) in between that of low and medium joint frequency

models; it is because the influence of shear strength along the joints is more in this model as the blocks are very close to each other. Runout obtained from the discrete model having high joint frequency is almost equal to runout obtained from the continuum model (Table 4). This agrees that as the joint frequency approaches infinity, a discrete system starts approaching a homogenous continuum system. Considering the longitudinal extent of the rock slope, small differences in the runout characteristics with the change in the modelling approach can be neglected.

7. CONCLUSIONS

The evolution of the Daguangbao landslide was analyzed in this study by using the novelly developed discrete and continuum numerical approaches. The final runout distance of 932m obtained from the developed discrete modelling approach generally agrees with the results (944m) achieved by DDA discontinuum modelling by Zhang et al. (2013). It validates the discontinuum analysis methodology employed in the present study. Furthermore, the displacement at the toe of the rockslide, evaluated per the CEL continuum model, was found to be on the lower side of the discrete modelling-based results. This is because dilatant phenomena like block rotation, separation, rolling, etc., cannot be simulated via continuum-based models.

Nevertheless, it was concluded that the post-failure geometry of the rockslide simulated from the continuum and discrete models is quite similar. Hence, these approaches can be utilized for the assessment of landslide runouts. Novelly, the effect of varying joint frequencies on the runout behaviour of landslides was also assessed in this work, and it was found that high joint frequencies correspond to lower landslide runout distances. Broadly, these modelling approaches were found not to be susceptible to significant variations based on the model parameters and hence can be relied upon for rockslide propagation analysis. In future, attempts must be made to study the effect of topography (out-of-plane direction) on the rockslide propagation in coupling with water.

Financial and Ethical Disclosures

The authors have no disclosures to declare.

Funding

This research study has received financial assistance from the “Deutscher Akademischer Austausch Dienst“(DAAD), Germany. The financial support is gratefully acknowledged. We also thank the “Institute of Geotechnics, University of Stuttgart” for providing the necessary physical resources for the research effort. We also thank the Institute of Eminence (IoE) for resources from the project code: PLN12/02CE, which was critical in carrying out this study.

Conflict of Interest

The authors have no conflict of interests to declare.

References

ABAQUS D. (2014). ABAQUS 6.14 Getting Started with Abaqus: Interactive Edition. ABAQUS 6.14 Getting Started, 693.

Bozzano F., Lenti L., Martino S., Montagna A., Paciello A. (2011). Earthquake triggering of landslides in highly jointed rock masses: Reconstruction of the 1783 Scilla rock avalanche (Italy). Geomorphology, 129(3-4):294–308.

Choi C.E., Cui Y., Liu L.H. D., Ng,C. W. W., Lourenço S.D.N. (2017). Impact mechanisms of granular flow against curved barriers. Géotechnique Letters, 7(4), 330–338.

Choi C.E., Ng, C.W.W., Law R.P.H., Song D., Kwan J.S.H., Ho K.K.S. (2015). Computational investigation of baffle configuration on impedance of channelized debris flow. Canadian Geotechnical Journal, 52(2):182–197.

Crosta G. B., IMPOSIMATO S., Roddeman D. G. (2006). Continuum numerical modelling of flow-like landslides. Landslides from Massive Rock Slope Failure, 211–232.

Cruden D. (1991). A simple definition of a landslide. Bulletin of the International Association of Engineering Geology, 43(1), 27–29.

Cundall P.A. (1971). A computer model for simulating progressive, large-scale movement in blocky rock system. Proceedings of the International Symposium on Rock Mechanics, 8:129–136.

Goel, R.K. and Mitra, S. (2015). Importance of weathering in rock engineering, Int Golden Jubilee Conf Engineering Geology in New Millennium EGNM-2015, Special Issue of Journal of Engineering Geology, October, New Delhi, pp.231-245.

Goel, R.K. and Mitra, S. (2021). Weathering and its Influence on Rock Slope, J of Rock Mech and Tunnelling Technology, Vol 27, No.1, pp.49-62.

GorumT., Fan X., van Westen C. J., Huang R.Q., Xu Q., Tang C., Wang G. (2011). Distribution pattern of earthquake-induced landslides triggered by 12 May 2008 Wenchuan earthquake. Geomorphology, 133(3–4):152–167.

Harp E.L., Jibson R.W. (1996). Landslides triggered by the 1994 Northridge, California, earthquake. Bulletin of the Seismological Society of America, 86(1B), S319–S332.

Hatzor Y.H., Feintuch A. (2001). The validity of dynamic block displacement prediction using DDA. International Journal of Rock Mechanics and Mining Sciences, 38(4):599–606.

Hoek E., Brown E. (1988). The Hoek-Brown failure criterion -a 1988 update. Toronto, 15.

Huang R., Pei X., Fan X., Zhang W., Li S., Li B. (2012). The characteristics and failure mechanism of the largest landslide triggered by the Wenchuan earthquake, May 12, 2008, China. Landslides, 9:131–142.

Huang R., Xu Q., Huo J. (2011). Mechanism and geo-mechanics models of landslides triggered by 5.12 Wenchuan earthquake. Journal of Mountain Science, 8:200–210.

Jibson R.W. (2011). Methods for assessing the stability of slopes during earthquakes—A retrospective. Engineering Geology, 122(1–2):43–50.

Kafaji I.K. (2013). Formulation of a dynamic material point method (MPM) for geomechanical problems, Doctoral Thesis, University of Stuttgart.

Keefer D.K. (2000). Statistical analysis of an earthquake-induced landslide distribution—The 1989 Loma Prieta, California event. Engineering Geology, 58(3):231–249.

Keefer D.K., Larsen M.C. (2007). Assessing landslide hazards. Science, 316(5828):1136–1138.

Kuo C.Y., Tai Y.C., Bouchut F., Mangeney A., Pelanti M., Chen RF., Chang, K.J. (2009). Simulation of Tsaoling landslide, Taiwan, based on Saint Venant equations over general topography. Engineering Geology, 104(3–4):181–189.

Kveldsvik V., Kaynia A. M., Nadim F., Bhasin R., Nilsen B., Einstein H.H. (2009). Dynamic distinct-element analysis of the 800 m high Åknes rock slope. International Journal of Rock Mechanics and Mining Sciences, 46(4):686–698.

Liu Y., Li H., Xiao K., Li J., Xia X., Liu B. (2014). Seismic stability analysis of a layered rock slope. Computers and Geotechnics, 55:474–481.

Manzella I., Labiouse V. (2013). Empirical and analytical analyses of laboratory granular flows to investigate rock avalanche propagation. Landslides, 10(1):23–36.

Moormann C., Hamad F., Shirole D. (2015). Seismic induced rock landslides using continuum-based models. In: Proc. ISRM Regional Symposium-EUROCK 2015.

Pirulli M. (2005). Numerical modelling of landslide runout, a continuum mechanics approach. Unpublished Ph. D. Dissertation, Politecnico Di Torino.

Pirulli M., Bristeau M.O., Mangeney A., Scavia C. (2007). The effect of the earth pressure coefficients on the runout of granular material. Environmental Modelling & Software, 22(10):1437–1454.

Qiu G., Henke S., Grabe J. (2009). Applications of Coupled Eulerian-Lagrangian method to geotechnical problems with large deformations. Proceeding of SIMULIA Customer Conference, 420-435.

Shi G., Goodman R.E. (1989). Generalization of two-dimensional discontinuous deformation analysis for forward modelling. International Journal for Numerical and Analytical Methods in Geomechanics, 13(4):359–380.

Shirole D., Walton G., Hedayat A. (2020a). Experimental investigation of multi-scale strain-field heterogeneity in rocks. International Journal of Rock Mechanics and Mining Sciences, 127:104212.

Sinha S., Shirole D., Walton G. (2020). Investigation of the Micromechanical Damage Process in a Granitic Rock Using an Inelastic Bonded Block Model (BBM). Journal of Geophysical Research: Solid Earth, 125(3), e2019JB018844.

Sinha S., Walton G. (2019). Understanding continuum and discontinuum models of rock-support interaction for excavations undergoing stress-induced spalling. International Journal of Rock Mechanics and Mining Sciences, 123, 104089.

Stead D., Eberhardt E., Coggan J. S. (2006). Developments in the characterization of complex rock slope deformation and failure using numerical modelling techniques. Engineering Geology, 83(1-3):217-235.

Varnes D.J. (1984). Landslide hazard zonation: A review of principles and practice, Natural Hazards, Issue No. 3, Publisher United Nations.

Wu J.H., Chen C.H. (2011). Application of DDA to simulate characteristics of the Tsaoling landslide. Computers and Geotechnics, 38(5):741-750.

Xu W.J., Xu Q., Wang Y.J. (2013). The mechanism of high-speed motion and damming of the Tangjiashan landslide. Engineering Geology, 157, 8-20.

Yueping Y., Yuliang C., Jun W., Meng W., Bin L.I.U., Yun S., Jingtao L. (2011). Remote sensing research on Daguangbao gigantic rockslide triggered by Wenchuan earthquake. Journal of Engineering Geology, 19(5):674–684.

Zhang Y., Chen G., Zheng L., Li Y., Wu J. (2013). Effects of near-fault seismic loadings on run-out of large-scale landslide: A case study. Engineering Geology, 166:216–236.